

GTA: A GEOMETRY-AWARE ATTENTION MECHANISM FOR MULTI-VIEW TRANSFORMERS

Takeru Miyato¹, Bernhard Jaeger¹, Max Welling², Andreas Geiger¹

{takeru.miyato, bernhard.jaeger, a.geiger}@uni-tuebingen.de
m.welling@uva.nl

¹ University of Tübingen, Tübingen AI Center

² University of Amsterdam

ABSTRACT

As transformers are equivariant to the permutation of input tokens, encoding the positional information of tokens is necessary for many tasks. However, since existing positional encoding schemes have been initially designed for NLP tasks, their suitability for vision tasks, which typically exhibit different structural properties in their data, is questionable. We argue that existing positional encoding schemes are suboptimal for 3D vision tasks, as they do not respect their underlying 3D geometric structure. Based on this hypothesis, we propose a geometry-aware attention mechanism that encodes the geometric structure of tokens as *relative transformation* determined by the geometric relationship between queries and key-value pairs. By evaluating on multiple novel view synthesis (NVS) datasets in the sparse wide-baseline multi-view setting, we show that our attention, called *Geometric Transform Attention (GTA)*, improves learning efficiency and performance of state-of-the-art transformer-based NVS models without any additional learned parameters and only minor computational overhead.

1 INTRODUCTION

The transformer model (Vaswani et al., 2017), which is composed of a stack of permutation symmetric layers, processes input tokens as a *set* and lacks direct awareness of the tokens’ structural information. Consequently, transformer models are not solely perceptible to the structures of input tokens, such as word order in NLP or 2D positions of image pixels or patches in image processing.

A common way to make transformers position-aware is through vector embeddings: in NLP, a typical way is to transform the position values of the word tokens into embedding vectors to be added to input tokens or attention weights (Vaswani et al., 2017; Shaw et al., 2018). While initially designed for NLP, these positional encoding techniques are widely used for 2D and 3D vision tasks today (Wang et al., 2018; Dosovitskiy et al., 2021; Sajjadi et al., 2022b; Du et al., 2023).

Here, a natural question arises: “Are existing encoding schemes suitable for tasks with very different geometric structures?”. Consider for example 3D vision tasks using multi-view images paired with camera transformations. The 3D Euclidean symmetry behind multi-view images is a more intricate structure than the 1D sequence of words. With the typical vector embedding approach, the model is tasked with uncovering useful camera poses embedded in the tokens and consequently struggles to understand the effect of non-commutative Euclidean transformations.

Our aim is to seek a principled way to incorporate the geometrical structure of the tokens into the transformer. To this end, we introduce a method that encodes the token relationships as transformations directly within the attention mechanism. More specifically, we exploit the relative transformation determined by the geometric relation between the query and the key-value tokens. We then apply those transformations to the key-value pairs, which allows the model to compute QKV attention in an aligned coordinate space.

The code and project page: <https://github.com/autonomousvision/gta>, <https://takeru.github.io/gta>.

We evaluate the proposed attention mechanism on several novel view synthesis (NVS) tasks with *sparse and wide-baseline* multi-view settings, which are particularly hard tasks where a model needs to learn *strong 3D geometric priors* from multiple training scenes. We show that existing positional encoding schemes are suboptimal and that our geometric-aware attention, named *geometric transform attention (GTA)*, significantly improves learning efficiency and performance of state-of-the-art transformer-based NVS models, just by replacing the existing positional encodings with GTA.

2 BACKGROUND

The transformer comprises attention modules as an essential building block. Given input token features $X \in \mathbb{R}^{n \times d}$, the attention layer’s output $O \in \mathbb{R}^{n \times d}$ is computed as follows:

$$O := \text{Attn}(Q, K, V) = \text{softmax}(QK^T)V, \quad (1)$$

where $Q, K, V = XW^Q, XW^K, XW^V \in \mathbb{R}^{n \times d}$, $W^{\{Q,K,V\}} \in \mathbb{R}^{d \times d}$, and (n, d) is the number of tokens and channel dimensions. Here, we omit the scale factor inside the softmax function for simplicity. X is assumed to be embeddings of a tokenized text sequence in NLP and image patches in 2D image processing. The output in Eq. (1) is invariant to the permutation of the key-value vector indices. This permutation symmetry needs to be broken, to make the attention aware of the token structure. In the context of NLP, where word order matters, positional information is encoded into the model through embeddings so that the model can make position-aware predictions. The original work of the transformer (Vaswani et al., 2017) incorporates the positional information as embeddings to be added to each input token. This encoding scheme is typically referred to as *absolute positional encoding* (APE), and APE-based attention can be written in the following form:

$$\text{softmax}((Q + \gamma(\mathbf{P})W^Q)(K + \gamma(\mathbf{P})W^K)^T)(V + \gamma(\mathbf{P})W^V), \quad (2)$$

where \mathbf{P} denotes the positional attributes of the tokens X and γ is a positional encoding function. From here, a bold symbol signifies that the corresponding variable consists of a list of elements. The typical choice for γ is the sinusoidal function, which transforms position values into Fourier features with multiple frequencies. A subsequent work (Shaw et al., 2018) proposes an alternative position-aware attention mechanism, which encodes the relative distance between each pair of query and key-value tokens as bias terms added to each component of the attention operation:

$$\text{softmax}(QK^T + \gamma_{\text{rel}}(\mathbf{P}))(V + \gamma'_{\text{rel}}(\mathbf{P})), \quad (3)$$

where $\gamma_{\text{rel}}(\mathbf{P}) \in \mathbb{R}^{n \times n}$ and $\gamma'_{\text{rel}}(\mathbf{P}) \in \mathbb{R}^{n \times d}$ are the bias terms that depend on the distance between tokens. This encoding scheme is called *relative positional encoding* (RPE) and ensures that the embeddings do not rely on the sequence length, with the aim of improving length generalization in the model.

Following the success in the field of NLP, transformers have demonstrated their efficacy on various image-based computer vision tasks (Wang et al., 2018; Ramachandran et al., 2019; Carion et al., 2020; Dosovitskiy et al., 2021; Ranftl et al., 2021; Romero & Cordonnier, 2021; Wu et al., 2021; Chitta et al., 2022). Those works use (variants of) APE or RPE applied to 2D positional information to make the model aware of 2D image structure, and the specific methodologies employed to integrate those embeddings vary across studies. Besides image-based vision tasks, there has been a surge of application of transformer-based models to 3D-vision (Wang et al., 2021; Liu et al., 2022; Kulhánek et al., 2022; Watson et al., 2023; Sajjadi et al., 2022b; Varma et al., 2023; Xu et al., 2023; Shao et al., 2023; Safin et al., 2023; Venkat et al., 2023; Du et al., 2023; Liu et al., 2023). In these works, APE or RPE is typically used to encode the geometric structure of input tokens into the model. For example, (Kulhánek et al., 2022; Watson et al., 2023; Du et al., 2023) embed the camera information by adding (linearly transformed) flattened camera extrinsic matrices to the patch tokens.

3 GEOMETRIC ENCODING BY RELATIVE TRANSFORMATION

In this work, we focus on novel view synthesis (NVS), which is a fundamental task in 3D-vision. The NVS task is to predict an image from a novel viewpoint, given a set of context views of a scene and their viewpoint information represented as 4×4 extrinsic matrices, each of which maps 3D

points in world coordinates to the respective points in camera coordinates. NVS tasks require the model to understand the scene geometry directly from raw image inputs.

Existing transformer-based NVS models use image patches from different viewpoints as image tokens and embed extrinsic matrices or ray information using an APE or RPE to inform the transformer of the viewpoint. Specifically, in Wang et al. (2021); Du et al. (2023), a linear transformation is applied to the flattened extrinsic matrix, which is subsequently added to the transformer’s input tokens. Sajjadi et al. (2022b) and Safin et al. (2023) use ray embeddings to inform the model of the token’s geometric information with APE- and RPE-based methods, respectively.

The main problem with this encoding of the camera transformation is that the essential operation in these positional encodings is *addition*: as we see in Eq. (2) and Eq. (3), the output of the embedding function is added to each token or to the attention matrix before the softmax function is applied. However, we know that the geometry behind multi-view images is governed by Euclidean symmetry. More specifically, when the viewpoint changes, the change of the object’s pose in the camera coordinates is computed based on the corresponding camera transformation.

Our proposed method incorporates geometric transformations directly into the transformer’s attention mechanism through a *relative transformation* of the QKV features. Specifically, each key-value token is transformed by a relative transformation that is determined by the geometric attributes between query and key-value tokens. This can be viewed as a coordinate system alignment, which has an analogy in geometric processing in computer vision: when comparing two sets of points each represented in a different camera coordinate space, we move one of the sets using a relative transformation cc'^{-1} to obtain all points represented in the same coordinate space. Here, c and c' are the extrinsics of the respective point sets. Our attention performs this coordinate alignment within the *attention feature space*. This alignment allows the model not only to compare query and key vectors in the same reference coordinate space, but also to perform the addition of the attention output at the residual path in the aligned local coordinates of each token due to the value vector’s transformation.

Group and representation: We briefly introduce the notion of a *group* and a *representation* because we describe our proposed attention through the language of group theory, which handles different geometric structures in a unified manner, such as camera transformations and image positions.

In short, a group, denoted as G with its element g , is an associative set that is closed under multiplication and has the identity element, with each element having an inverse. For example, the set of camera transformations satisfies the axiom of a group and is called *special Euclidean group*: $SE(3)$.

A (real) *representation* is a function $\rho : G \rightarrow GL_d(\mathbb{R})$ such that $\rho(g)\rho(g') = \rho(gg')$ for any $g, g' \in G$. Here, $GL_d(\mathbb{R})$ denotes the set of $d \times d$ invertible real-valued matrices. We denote by $\rho_g := \rho(g) \in \mathbb{R}^{d \times d}$ a representation of g . A simple choice for the representation ρ_g for $g \in SE(3)$ is a homogeneous rigid transformation matrix $\begin{bmatrix} R & T \\ 0 & 1 \end{bmatrix} \in \mathbb{R}^{4 \times 4}$ where $R \in \mathbb{R}^{3 \times 3}$ is a 3D rotation matrix and $T \in \mathbb{R}^{3 \times 1}$ is a 3D translation. A block concatenation of multiple group representations is also a representation. What representation to use is the user’s choice. We will present different design choices of ρ for several NVS applications in Section 3.1 and 3.2.

3.1 GEOMETRIC TRANSFORM ATTENTION

Suppose that we have a set of token features $X \in \mathbb{R}^{n \times d}$ and a list of geometric attributes $\mathbf{g} = [g_1, \dots, g_n]$, where g_i is an i -th token’s geometric attribute represented as a group element. For example, each X_i corresponds to a patch feature or an RGB value, and g_i corresponds to a camera transformation and an image position. Given a representation ρ and $Q, K, V = XW^Q, XW^K, XW^V \in \mathbb{R}^{n \times d}$, we define our geometry-aware attention given query Q_i as follows:

$$O_i = \sum_j^n \frac{\exp(Q_i^T (\rho_{g_i g_j^{-1}} K_j))}{\sum_{j'=1}^n \exp(Q_i^T (\rho_{g_i g_{j'}^{-1}} K_{j'}))} (\rho_{g_i g_j^{-1}} V_j). \quad (4)$$

Using $\rho_{g_i g_j^{-1}} = \rho_{g_i} \rho_{g_j^{-1}}$, the above equation can be transformed into the following form:

$$O_i = \rho_{g_i} \sum_j^n \frac{\exp((\rho_{g_i}^T Q_i)^T (\rho_{g_j^{-1}} K_j))}{\sum_{j'=1}^n \exp((\rho_{g_i}^T Q_i)^T (\rho_{g_{j'}^{-1}} K_{j'}))} (\rho_{g_j^{-1}} V_j). \quad (5)$$

Note that the latter expression is computationally and memory-wise more efficient, requiring computation and storage of n^2 values of each $(\rho_{g_i g_j^{-1}} K_j, \rho_{g_i g_j^{-1}} V_j)$ in Eq. (4) versus only n values for $(\rho_{g_i}^T Q_i, \rho_{g_j}^{-1} K_j, \rho_{g_j}^{-1} V_j)$ and $\rho_{g_i} \hat{O}_i$ in Eq. (5), where \hat{O}_i is the output of the leftmost sum.

Eq. (5), given all queries Q , can be compactly rewritten in an implementation-friendly form:

$$\mathbf{P}_g \odot \text{Attn} \left(\mathbf{P}_g^T \odot Q, \mathbf{P}_g^{-1} \odot K, \mathbf{P}_g^{-1} \odot V \right), \quad (6)$$

where \mathbf{P}_g denotes a list of representations for different tokens: $\mathbf{P}_g := [\rho_{g_1}, \dots, \rho_{g_n}]$, and “ \odot ” denotes token-wise matrix multiplication: $\mathbf{P}_g \cdot K = [\rho_{g_1} K_1 \cdots \rho_{g_n} K_n]^T \in \mathbb{R}^{n \times d}$. Also, the transpose T and the inverse $^{-1}$ operate element-wise on \mathbf{P}_g : $\mathbf{P}_g^T := [\rho_{g_1}^T, \dots, \rho_{g_n}^T]$ and $\mathbf{P}_g^{-1} := [\rho_{g_1}^{-1}, \dots, \rho_{g_n}^{-1}]$. We call the attention mechanism in Eq. (6) *geometric transform attention (GTA)*. Note that the additional computation of GTA is smaller than the QKV attention and the feedforward MLP in the transformer when constructing ρ_g from a set of small matrices, which we will detail in Section 3.2. Appendix A provides the computation overhead of the “ $\mathbf{P} \odot$ ” operation, as well as an algorithmic description of GTA.

A simple NVS experiment: We first demonstrate that GTA improves the learning efficiency compared to APE- and RPE-based positional encodings in a simplified novel view synthesis experiment. We construct a setting where only camera rotations are relevant to show that the complexity of the representation ρ_g can be adapted to the problem complexity. A single empty scene surrounded by an enclosing sphere whose texture is shown in Fig. 1 left is considered. All cameras are placed in the center of the scene where they can be rotated but not translated. Each scene consists of 8 context images with 32x32 pixel resolution rendered with a pinhole camera model. The camera poses are chosen by randomly sampling camera rotations. We randomize the global coordinate system by setting it to the first input image. This increases the difficulty of the task and is similar to standard NVS tasks, where the global origin may be placed anywhere in the scene by camera pose estimation methods like COLMAP (Schönberger & Frahm, 2016). The goal is to render a target view given its camera extrinsic and a set of context images.

We employ a transformer-based encoder-decoder architecture shown on the right of Fig. 1. Camera extrinsics in this synthetic experiment form the 3D rotation group: $SO(3)$. Therefore, we choose ρ_g to be a block concatenation of the 3×3 camera rotation matrix: $\rho_{g_i} := \underbrace{R_i \oplus \cdots \oplus R_i}_{d/3 \text{ times}}$ where R_i is

the 3×3 matrix representation of the extrinsic $g_i \in SO(3)$ linked to the i -th token. Here, $A \oplus B$ denotes block-concatenation: $A \oplus B = \begin{bmatrix} A & 0 \\ 0 & B \end{bmatrix}$. The number of channels d used in the transformer needs to be divisible by 3. We set d to 510.

We compare this model to APE- and RPE-based transformers as baselines. For the APE-based transformer, we add each flattened rotation matrix associated with each token to each attention layer’s input. Since we could not find an RPE-based method that is directly applicable to our setting with rotation matrices, we use an RPE-version of our attention where instead of multiplying the matrices with the QKV features, we apply the matrices to *biases*. More specifically, for each head, we prepare learned bias vectors $b^Q, b^K, b^V \in \mathbb{R}^9$ concatenated with each of the QKV vectors of each head and apply the representation matrix defined by $\rho(g) := R \oplus R \oplus R \in \mathbb{R}^{9 \times 9}$, only to the bias vectors. This model can bias the attention matrix by the Frobenius inner product of rotation matrices, which is a natural inner product of matrices that we describe in more detail in Appendix B.

Fig. 2 on the left shows that the GTA-based transformer outperforms both the APE and RPE-based transformers in terms of both training and test performance. In Fig. 2 on the right, the GTA-based transformer reconstructs the image structure better than the other positional encoding schemes.

3.2 TOKEN STRUCTURE AND DESIGN OF REPRESENTATION ρ FOR NVS

In the previous synthetic experiment, tokens were simplified to comprise an entire image feature and an associated camera extrinsic. This differs from typical NVS model token structures, like those in (Sajjadi et al., 2022b; Du et al., 2023), where patched image tokens are used, and each of the tokens can be linked not only to a camera transformation but also to a 2D location within an image. To adapt GTA to such NVS models, we now describe how we associate each feature with a geometric attribute and outline one specific design choice for ρ .

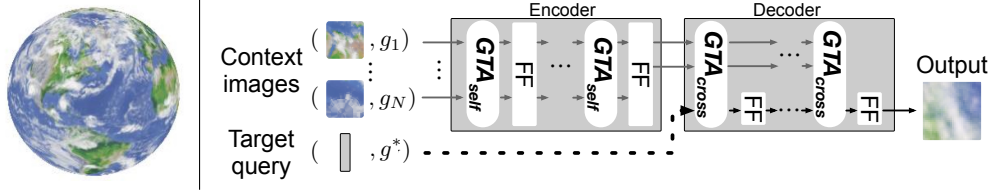


Figure 1: **Synthetic experiment.** Left: Texture of the surrounding sphere. Right: Model architecture. The query pair consists of a learned constant value and a target extrinsic g^* .

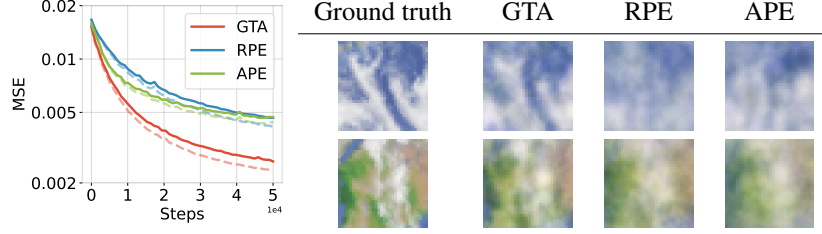


Figure 2: **Results on the synthetic dataset.** Left: The solid and dashed lines indicate test and train errors. Right: Patches predicted with different positional encoding schemes.

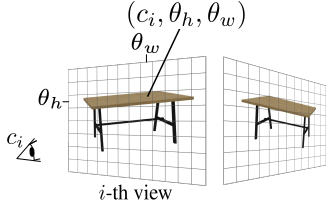


Figure 3: Geometric attributes.

Token structure: We follow a common way to compose the input tokens for the transformer as in (Sajjadi et al., 2022b; Du et al., 2023). We assume that for each view, we have image patches or pixels of the size of $H \times W$, and each patch or pixel token consists of a pair of a feature value $x \in \mathbb{R}^d$ and geometric attributes that are a 4×4 camera extrinsic $c \in SE(3)$ and a 2D image position. For image positional encoding, it would be natural to encode each position as an element of the 2D translation group $T(2)$. However, we found, similarly to the Fourier feature embeddings used in APE and RPE and rotary positional encoding (Su et al., 2021), encoding the image positions as elements of the 2D rotation group $SO(2)$ exhibits better performance than using $T(2)$. Thus, we represent each 2D image position as an element of the direct product of the two $SO(2)$ groups: $(\theta_h, \theta_w) \in SO(2) \times SO(2)$ where $\theta_h, \theta_w \in [0, 2\pi)$. Here, we identify the $SO(2)$ element with the 2D rotation angle. We associate the top left patch (or pixel) with the value $(0, 0)$, while the bottom right patch corresponds to $(2\pi(H-1)/H, 2\pi(W-1)/W)$. For the intermediate patches, we compute their values using linear interpolation of the angle values between the top left and bottom right patches. Overall, we represent the geometric attribute of each token of the i -th view by

$$g := (c_i, \theta_h, \theta_w) \in SE(3) \times SO(2) \times SO(2) =: G. \quad (7)$$

Fig. 3 illustrates how we represent each geometric attribute of each token.

Design of ρ : What representation to use is a design choice similar to the design choice of the embedding in APE and RPE. As a specific design choice for the representation for NVS tasks, we propose to compose ρ_g by the direct sum of multiple irreducible representation matrices, each

Table 1: **Components of ρ_g .**

	$\sigma_{\text{cam}}(c)$	$\sigma_{\text{rot}}(r)$	$\sigma_h(\theta_h)$	$\sigma_w(\theta_w)$
matrix form	$\begin{bmatrix} R & T \\ 0 & 1 \end{bmatrix}$	$\begin{bmatrix} D_r^{(l_1)} & & \\ & \ddots & \\ & & D_r^{(l_{N_{\text{rot}}})} \end{bmatrix}$	$\begin{bmatrix} M_{\theta_h}^{(f_1)} & & \\ & \ddots & \\ & & M_{\theta_h}^{(f_{N_h})} \end{bmatrix}$	$\begin{bmatrix} M_{\theta_w}^{(f_1)} & & \\ & \ddots & \\ & & M_{\theta_w}^{(f_{N_w})} \end{bmatrix}$
multiplicity	s	t	u	v

Table 2: **Test metrics.** Left: CLEVR-TR, Right: MSN-Hard. LFN and PixelNeRF are trained and evaluated on MultiShapeNet, not MSN-Hard. They are different datasets but generated from an identical distribution.

	PSNR↑		PSNR↑	LPIPS ↓	SSIM↑
APE	33.66	LFN (Sitzmann et al., 2021)	14.77	0.582	0.328
RPE	36.08	PixelNeRF (Yu et al., 2021)	21.97	0.332	0.689
SRT	33.51	SRT (Sajjadi et al., 2022b)	24.27	0.368	0.741
RePAST	37.27	RePAST (Safin et al., 2023)	24.48	0.348	0.751
GTA (Ours)	39.63	GTA (Ours)	25.72	0.289	0.798

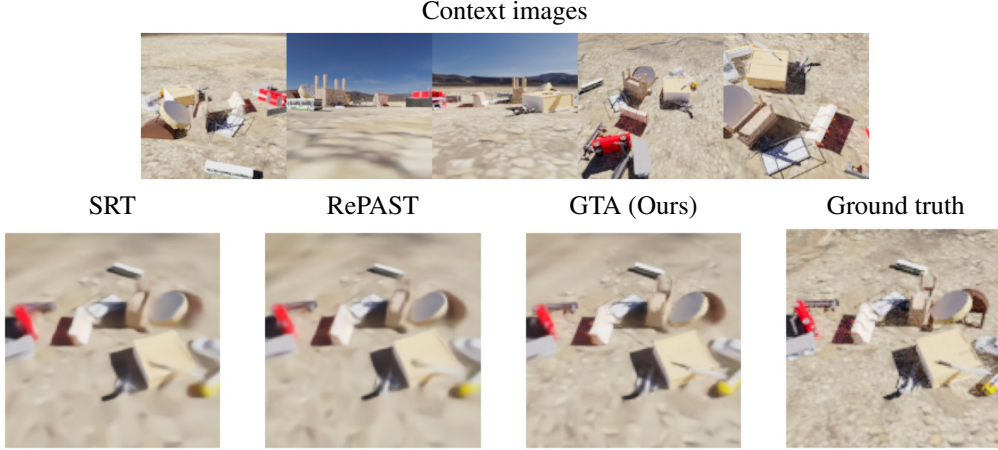


Figure 4: **Qualitative results on MSN-Hard.**

responding to a specific component of the group G . Specifically, ρ_g is composed of four different types of representations and is expressed in block-diagonal form as follows:

$$\rho_g := \sigma_{\text{cam}}^{\oplus s}(c) \oplus \sigma_{\text{rot}}^{\oplus t}(r) \oplus \sigma_h^{\oplus u}(\theta_h) \oplus \sigma_w^{\oplus v}(\theta_w), \text{ where } A^{\oplus a} = \underbrace{A \oplus \dots \oplus A}_{a \text{ times}}. \quad (8)$$

Here, “ \oplus ” denotes block-concatenation $A \oplus B = \begin{bmatrix} A & 0 \\ 0 & B \end{bmatrix}$. We introduce an additional representation $\sigma_{\text{rot}}(r)$ that captures only the rotational information of c , with which we find moderate improvements in performance. Table 1 summarizes the matrix form we use for each representation.

Specifically, $M_\theta^{(f)}$ is a 2D rotation matrix with frequency f that is analogous to the frequency parameter used in Fourier feature embeddings in APE and RPE. $D_r^{(l)}$ can be thought of as the 3D version of $M_\theta^{(f)}$. Please refer to Appendix C for more detailed descriptions of these matrices. Fig. 8 in the Appendix displays the actual representation matrices used in our experiments.

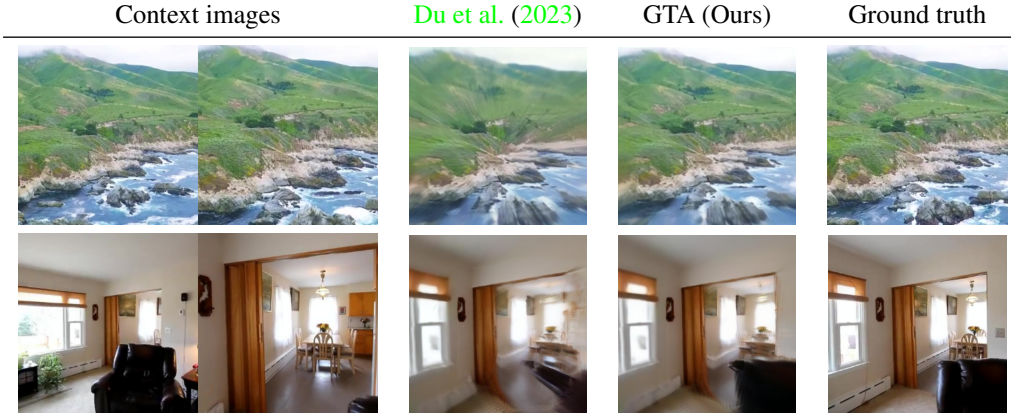
4 EXPERIMENTAL EVALUATION

We conducted experiments on several sparse NVS tasks to evaluate GTA and compare the reconstruction quality with different positional encoding schemes as well as existing NVS methods.

Datasets: We evaluate our method on two synthetic 360° datasets with sparse and wide baseline views (*CLEVR-TR* and *MSN-Hard*) and on two datasets of real scenes with distant views (*RealEstate10k* and *ACID*). We train a separate model for each dataset and describe the properties of each dataset below. *CLEVR* with translation and rotation (*CLEVR-TR*) is a multi-view version of *CLEVR* (Johnson et al., 2017) that we propose. It features scenes with randomly arranged basic objects captured by cameras with azimuth, elevation, and translation transformations. We use this dataset to measure the ability of models to understand the underlying geometry of scenes. We set the number of context views to 2 for this dataset. Generating 360° images from 2 context views is

Table 3: **Results on RealEstate10k and ACID.**

	RealEstate10k			ACID		
	PSNR \uparrow	LPIPS \downarrow	SSIM \uparrow	PSNR \uparrow	LPIPS \downarrow	SSIM \uparrow
PixelNeRF (Yu et al., 2021)	13.91	0.591	0.460	16.48	0.628	0.464
IBRNet (Wang et al., 2021)	15.99	0.532	0.484	19.24	0.385	0.513
GPNR (Suhail et al., 2022)	18.55	0.459	0.748	17.57	0.558	0.719
Du et al. (2023)	21.65	0.285	0.822	23.35	0.334	0.801
GTA (Ours)	22.85	0.255	0.850	24.10	0.291	0.824

Figure 5: **Qualitative results.** Top: ACID, Bottom: RealEstate10k.

challenging because parts of the scene will be unobserved. The task is solvable because all rendered objects have simple shapes and textures. This allows models to infer unobserved regions if they have a good understanding of the scene geometry. MultiShapeNet-Hard (MSN-Hard) is a challenging dataset introduced in Sajjadi et al. (2022a;b). Up to 32 objects appear in each scene and are drawn from 51K ShapeNet objects (Chang et al., 2015), each of which can have intricate textures and shapes. Each view is captured from a camera pose randomly sampled from 360° viewpoints. Objects in test scenes are withheld during training. MSN-Hard assesses both the understanding of complex scene geometry and the capability to learn strong 3D object priors. Each scene has 10 views, and following Sajjadi et al. (2022a;b), we use 5 views as context views and the remaining views as target views. RealEstate10k (Zhou et al., 2018) consists of real indoor and outdoor scenes with estimated camera parameters. ACID (Liu et al., 2021) is similar to RealEstate10k, but solely includes outdoor scenes. Following Du et al. (2023), during training, we randomly select two context views and one intermediate target view per scene. At test time, we sample distant context views with 192 time-step intervals and evaluate the reconstruction quality of intermediate views.

Baselines: Scene representation transformer (SRT) (Sajjadi et al., 2022b), a transformer-based NVS method, serves as our baseline model on CLEVR-TR and MSN-Hard. SRT is a similar architecture to the one we describe in Fig. 1, but instead of the extrinsic matrices, SRT encodes the ray information into the architecture by concatenating Fourier feature embeddings of rays to the input pixels of the encoder. SRT is an APE-based model. Details of the SRT rendering process are provided in Appendix D.1 and Fig. 9. We also train another more recent transformer-based NVS model called RePAST (Safin et al., 2023). This model is a variant of SRT and encodes ray information via an RPE scheme, where, in each attention layer, the ray embeddings are added to the query and key vectors. The rays linked to the queries and keys are transformed with the extrinsic matrix associated with a key-value token pair, before feeding them into the harmonic embedding functions, to represent both rays in the same coordinate system. RePAST is the current state-of-the-art method on MSN-Hard. The key difference between GTA and RePAST is that the relative transformation is applied directly to QKV features in GTA, while it is applied to rays followed by harmonic embeddings in RePAST.

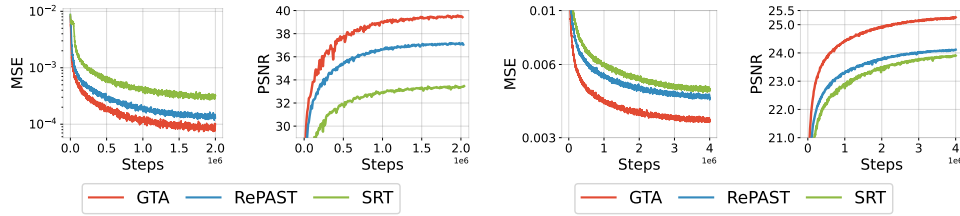


Figure 6: **Training and validation curves.** Left: CLEVR-TR, Right: MSN-Hard.

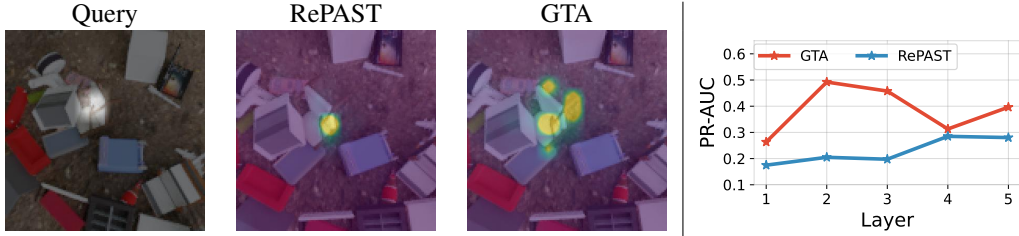


Figure 7: **Attention analysis.** Given a query token (white region), the attention weights on a context view are visualized. GTA can identify the shape of the object that corresponds to the given query. Right: Quantitative evaluation of alignments between attention matrices and object masks.

For RealEstate10k and ACID, we use the model proposed in [Du et al. \(2023\)](#), which is the state-of-the-art model on those datasets, as our baseline. Their model is similar to SRT, but has architectural improvements and uses a different token sampling strategy. The model encodes extrinsic matrices and 2D image positions to the encoder via APE, and also encodes rays associated with each query and context image patch token in the decoder via APE.

We implement our model by extending those baselines. Specifically, we replace all attention layers in both the encoder and decoder with GTA and remove any vector embeddings of rays, extrinsic matrices, and image positions from the model. We train our models and baselines with the same settings within each dataset. We train each model for 2M and 4M iterations on CLEVR-TR and MSH-Hard and for 300K iterations on both RealEstate10k and ACID, respectively. We report the reproduced numbers of baseline models in the main tables and show comparisons between the reported values and our reproduced results in Table 8 and Table 9 in Appendix D. Please also see Appendix D for more details about our experimental settings.

Results: Tables 2 and 3 show that GTA improves the baselines in all reconstruction metrics on all datasets. Fig. 4 shows that on MSN-Hard, the GTA-based model renders sharper images with more accurate reconstruction of object structures than the baselines. Fig. 5 shows that our GTA-based transformer further improves the geometric understanding of the scenes over [Du et al. \(2023\)](#) as evidenced by the sharper results and the better recovered geometric structures. Additional rendered images are provided in the Appendix (Figures 14-17). Videos are provided in the supplemental material. We also train models, encoding 2D positions and camera extrinsics via APE and RPE, to directly compare these encodings with GTA. See Appendix D.3 for details. Table 2 on the left shows that GTA outperforms APE and RPE on CLEVR-TR.

Fig. 6 shows that GTA-based models improve learning efficiency over SRT and RePAST by a significant margin and reach the same performance as RePAST using only around one-fifth and one-sixth of the training steps on CLEVR-TR and MSN-Hard. Our model also outperforms RePAST in terms of wall-clock time as each gradient update step is slightly faster than that of RePAST, see also Table 12 in Appendix E.4.

Object localization: As demonstrated in Fig. 7 on MSN-Hard, the GTA-based transformer not only correctly finds patch-to-patch associations but also recovers *patch-to-object* associations already in the second attention layer of the encoder. For quantitative evaluation, we compute precision-recall-AUC (PR-AUC) scores based on object masks provided by MSN-Hard. In short, the score represents, given a query token belonging to a certain object instance, how well the attention matrix aligns with the object masks across all context views. Details on how we compute PR-AUC are provided in Appendix E.3. The PR-AUCs for the second attention layer are 0.492 and 0.204 with GTA and

Table 4: **Ablation study.** All numbers show test PSNRs and are produced with models trained for 1M iterations, both for CLEVR-TR and MSN-Hard.

(a) Parentheses indicate that representations are not used in the encoder. Camera and image position are necessary in the decoder to identify which pixel to render.

$SE(3)$	$SO(2)$	$SO(3)$	CLEVR-TR	MSN-Hard
✓	(✓)		37.45	20.33
(✓)	✓		38.26	23.82
✓	✓		38.99	24.58
✓	✓	✓	39.00	24.80

(b) Performance of different representations encoding image positions. *A single frequency is used.

	CLEVR-TR	MSN-Hard
$SE(3) + T(2)$	37.20	23.69
$SE(3) + SO(2)^*$	38.82	23.98
$SE(3) + SO(2)$	38.99	24.58

RePAST, respectively, which demonstrates that our GTA-based transformer quickly identifies where to focus attention at the object level.

Representation design: Table 4a shows that, without camera encoding ($SE(3)$) or image positional encoding ($SO(2)$) in the encoder, the reconstruction quality degrades, showing that both representations are helpful in aggregating multi-view features. Using $SO(3)$ representations causes a moderate improvement on MSN-Hard and no improvement on CLEVR-TR. A reason for this could be that MSN-Hard consists of a wide variety of objects. By using the $SO(3)$ representation, which is invariant to camera translations, the model may be able to encode object-centric features more efficiently. Table 4b confirms that similar to Fourier feature embeddings used in APE and RPE, multiple frequencies of the $SO(2)$ representations benefit the reconstruction quality.

5 RELATED WORKS

Our newly proposed attention module shares its philosophy with the classic transformation autoencoder (Hinton et al., 2011; Cohen & Welling, 2014; Worrall et al., 2017; Rhodin et al., 2018; Falorsi et al., 2018; Chen et al., 2019) and recent equivariant representation learning models (Park et al., 2022; Miyato et al., 2022; Koyama et al., 2023). In these works, geometric information is provided as a transformation. Suppose $\Phi(x)$ is an encoded feature, where Φ is a nonlinear function such as a neural network, and g is an associated group element (e.g. rotation). Then the pair $(\Phi(x), g)$ is identified with $\rho_{g^{-1}}\Phi(x)$. Our proposed attention integrates this *feature transformation* into the attention mechanism as a way to break the permutation symmetry of the transformer architecture.

Rotary positional embeddings (Su et al., 2021; Sun et al., 2022) are similar to the $SO(2)$ representations in GTA. An interesting difference to the proposed mechanism is that the rotary positional embedding only applies transformations to query and key vectors, and not on the value vectors. In our setting, this exclusion leads to a discrepancy between the coordinate system of the key and value vectors, both of which interact with the tokens from which the query vectors are derived. Table 5 shows that removing the transformation on the value vectors leads to a significant drop in performance. The representations in this experiment do not include the $SO(3)$ component.

Table 5: **Effect of ρ_g on V .**

	CLEVR-TR	MSN-Hard
No ρ_g on V	36.54	23.77
GTA	38.99	24.58

The gauge transform used in gauge equivariant networks (Cohen et al., 2019; De Haan et al., 2021; He et al., 2021; Brandstetter et al., 2022) is also related to the relative transform used in our attention mechanism. However, the equivariant models and ours differ because they are built on different motivations. In short, the gauge equivariant layers are built to preserve the feature field structure determined by a gauge transformation. In contrast, our model applies the relative transform only on the query and key-value pair in the attention mechanism but does not impose equivariance on the weight matrices of the attention and the feedforward layers. The relative transformation in GTA can be thought of as a form of guidance that helps the model learn structured features within the attention mechanism from the initially unstructured raw multi-view images.

6 CONCLUSION

We have proposed a novel geometry-aware attention mechanism for transformers and demonstrated its efficacy by applying it to sparse wide-baseline novel view synthesis tasks. A limitation of GTA is that GTA and general positional encoding schemes rely on known poses or poses estimated by other algorithms, such as COLMAP (Schönberger & Frahm, 2016). An interesting future direction is to simultaneously learn the geometric information together with the forward propagation of features in the transformer. Developing an algorithm capable of autonomously acquiring such structural information solely from observations, specifically seeking a *universal learner* for diverse forms of structure akin to human capacity, represents a captivating avenue for future research.

7 ACKNOWLEDGEMENT

Takeru Miyato, Bernhard Jaeger, and Andreas Geiger were supported by the ERC Starting Grant LEGO-3D (850533) and the DFG EXC number 2064/1 - project number 390727645. The authors thank the International Max Planck Research School for Intelligent Systems (IMPRS-IS) for supporting Bernhard Jaeger. We thank Mehdi Sajjadi and Yilun Du for their comments and guidance on how to reproduce the results and thank Karl Stelzner for his reproducing code for the SRT models. We also thank Haoyu He, Haoqi Xu, Gege Gao, Masanori Koyama, Kashyap Chitta, and Naama Pearl for their feedback and comments. Takeru Miyato acknowledges his affiliation with the ELLIS (European Laboratory for Learning and Intelligent Systems) PhD program.

REFERENCES

- Johannes Brandstetter, Rob Hesselink, Elise van der Pol, Erik J Bekkers, and Max Welling. Geometric and physical quantities improve E(3) equivariant message passing. In *Proc. of the International Conf. on Learning Representations (ICLR)*, 2022. 9
- Nicolas Carion, Francisco Massa, Gabriel Synnaeve, Nicolas Usunier, Alexander Kirillov, and Sergey Zagoruyko. End-to-end object detection with transformers. In *Proc. of the European Conf. on Computer Vision (ECCV)*, 2020. 2
- Angel X. Chang, Thomas Funkhouser, Leonidas Guibas, Pat Hanrahan, Qixing Huang, Zimo Li, Silvio Savarese, Manolis Savva, Shuran Song, Hao Su, Jianxiong Xiao, Li Yi, and Fisher Yu. ShapeNet: An Information-Rich 3D Model Repository. Technical Report arXiv:1512.03012 [cs.GR], Stanford University — Princeton University — Toyota Technological Institute at Chicago, 2015. 7, 15
- Xu Chen, Jie Song, and Otmar Hilliges. Monocular neural image based rendering with continuous view control. In *Proc. IEEE Conf. on Computer Vision and Pattern Recognition (CVPR)*, pp. 4090–4100, 2019. 9
- Gregory S Chirikjian. *Engineering applications of noncommutative harmonic analysis: with emphasis on rotation and motion groups*. CRC press, 2000. 15
- Kashyap Chitta, Aditya Prakash, Bernhard Jaeger, Zehao Yu, Katrin Renz, and Andreas Geiger. Transfuser: Imitation with transformer-based sensor fusion for autonomous driving. *IEEE Trans. on Pattern Analysis and Machine Intelligence (PAMI)*, 2022. 2
- Taco Cohen, Maurice Weiler, Berkay Kicanaoglu, and Max Welling. Gauge equivariant convolutional networks and the icosahedral cnn. In *Proc. of the International Conf. on Machine learning (ICML)*, pp. 1321–1330, 2019. 9
- Taco S Cohen and Max Welling. Transformation properties of learned visual representations. In *Proc. of the International Conf. on Learning Representations (ICLR)*, 2014. 9
- Pim De Haan, Maurice Weiler, Taco Cohen, and Max Welling. Gauge equivariant mesh cnns: Anisotropic convolutions on geometric graphs. In *Proc. of the International Conf. on Learning Representations (ICLR)*, 2021. 9
- Alexey Dosovitskiy, Lucas Beyer, Alexander Kolesnikov, Dirk Weissenborn, Xiaohua Zhai, Thomas Unterthiner, Mostafa Dehghani, Matthias Minderer, Georg Heigold, Sylvain Gelly, Jakob Uszkoreit, and Neil Houlsby. An image is worth 16x16 words: Transformers for image recognition at scale. In *Proc. of the International Conf. on Learning Representations (ICLR)*, 2021. 1, 2

- Yilun Du, Cameron Smith, Ayush Tewari, and Vincent Sitzmann. Learning to render novel views from wide-baseline stereo pairs. In *Proc. IEEE Conf. on Computer Vision and Pattern Recognition (CVPR)*, pp. 4970–4980, 2023. 1, 2, 3, 4, 5, 7, 8, 16, 17, 18, 19, 20, 21, 25, 26
- Luca Falorsi, Pim de Haan, Tim R Davidson, Nicola De Cao, Maurice Weiler, Patrick Forré, and Taco S Cohen. Explorations in homeomorphic variational auto-encoding. *arXiv.org*, 2018. 9
- Klaus Greff, Francois Belletti, Lucas Beyer, Carl Doersch, Yilun Du, Daniel Duckworth, David J Fleet, Dan Gnanapragasam, Florian Golemo, Charles Herrmann, Thomas Kipf, Abhijit Kundu, Dmitry Lagun, Issam Laradji, Hsueh-Ti (Derek) Liu, Henning Meyer, Yishu Miao, Derek Nowrouzezahrai, Cengiz Oztireli, Etienne Pot, Noha Radwan, Daniel Rebain, Sara Sabour, Mehdi S. M. Sajjadi, Matan Sela, Vincent Sitzmann, Austin Stone, Deqing Sun, Suhani Vora, Ziyu Wang, Tianhao Wu, Kwang Moo Yi, Fangcheng Zhong, and Andrea Tagliasacchi. Kubric: a scalable dataset generator. In *CVPR*, 2022. 15
- Lingshen He, Yiming Dong, Yisen Wang, Dacheng Tao, and Zhouchen Lin. Gauge equivariant transformer. In *Advances in Neural Information Processing Systems (NeurIPS)*, pp. 27331–27343, 2021. 9
- Geoffrey E Hinton, Alex Krizhevsky, and Sida D Wang. Transforming auto-encoders. In *Proc. of the International Conf. on Artificial Neural Networks (ICANN)*, pp. 44–51, 2011. 9
- Justin Johnson, Bharath Hariharan, Laurens van der Maaten, Li Fei-Fei, C Lawrence Zitnick, and Ross Girshick. Clevr: A diagnostic dataset for compositional language and elementary visual reasoning. In *Proc. IEEE Conf. on Computer Vision and Pattern Recognition (CVPR)*, pp. 1988–1997, 2017. 6
- Masanori Koyama, Kenji Fukumizu, Kohei Hayashi, and Takeru Miyato. Neural fourier transform: A general approach to equivariant representation learning. *arXiv.org*, 2023. 9
- Jonáš Kulháněk, Erik Derner, Torsten Sattler, and Robert Babuška. Viewformer: Nerf-free neural rendering from few images using transformers. In *Proc. of the European Conf. on Computer Vision (ECCV)*, pp. 198–216, 2022. 2
- Andrew Liu, Richard Tucker, Varun Jampani, Ameesh Makadia, Noah Snaveley, and Angjoo Kanazawa. Infinite nature: Perpetual view generation of natural scenes from a single image. In *Proceedings of the IEEE/CVF International Conference on Computer Vision*, pp. 14458–14467, 2021. 7
- Ruoshi Liu, Rundu Wu, Basile Van Hoorick, Pavel Tokmakov, Sergey Zakharov, and Carl Vondrick. Zero-1-to-3: Zero-shot one image to 3d object. *arXiv.org*, 2023. 2
- Yingfei Liu, Tiancai Wang, Xiangyu Zhang, and Jian Sun. Petr: Position embedding transformation for multi-view 3d object detection. In *Proc. of the European Conf. on Computer Vision (ECCV)*, pp. 531–548. Springer, 2022. 2
- Ilya Loshchilov and Frank Hutter. Decoupled weight decay regularization. *arXiv.org*, 1711.05101, 2017. 14, 16
- Takeru Miyato, Masanori Koyama, and Kenji Fukumizu. Unsupervised learning of equivariant structure from sequences. In *Advances in Neural Information Processing Systems (NeurIPS)*, pp. 768–781, 2022. 9
- Jung Yeon Park, Ondrej Biza, Linfeng Zhao, Jan Willem van de Meent, and Robin Walters. Learning symmetric embeddings for equivariant world models. In *Proc. of the International Conf. on Machine Learning (ICML)*, pp. 17372–17389, 2022. 9
- Prajit Ramachandran, Niki Parmar, Ashish Vaswani, Irwan Bello, Anselm Levskaya, and Jon Shlens. Stand-alone self-attention in vision models. *Advances in Neural Information Processing Systems (NeurIPS)*, pp. 68–80, 2019. 2
- René Ranftl, Alexey Bochkovskiy, and Vladlen Koltun. Vision transformers for dense prediction. In *Proc. of the IEEE International Conf. on Computer Vision (ICCV)*, pp. 12179–12188, 2021. 2, 18
- Helge Rhodin, Mathieu Salzmann, and Pascal Fua. Unsupervised geometry-aware representation for 3D human pose estimation. In *Proc. of the European Conf. on Computer Vision (ECCV)*, pp. 750–767, 2018. 9
- David W Romero and Jean-Baptiste Cordonnier. Group equivariant stand-alone self-attention for vision. In *Proc. of the International Conf. on Learning Representations (ICLR)*, 2021. 2
- Aleksandr Safin, Daniel Duckworth, and Mehdi SM Sajjadi. RePAST: Relative pose attention scene representation transformer. *arXiv.org*, 2023. 2, 3, 6, 7, 17

- Mehdi SM Sajjadi, Daniel Duckworth, Aravindh Mahendran, Sjoerd van Steenkiste, Filip Pavetić, Mario Lučić, Leonidas J Guibas, Klaus Greff, and Thomas Kipf. Object scene representation transformer. In *Advances in Neural Information Processing Systems (NeurIPS)*, pp. 9512–9524, 2022a. 7, 16
- Mehdi SM Sajjadi, Henning Meyer, Etienne Pot, Urs Bergmann, Klaus Greff, Noha Radwan, Suhani Vora, Mario Lučić, Daniel Duckworth, Alexey Dosovitskiy, et al. Scene representation transformer: Geometry-free novel view synthesis through set-latent scene representations. In *Proc. IEEE Conf. on Computer Vision and Pattern Recognition (CVPR)*, pp. 6229–6238, 2022b. 1, 2, 3, 4, 5, 6, 7, 17
- Johannes Lutz Schönberger and Jan-Michael Frahm. Structure-from-motion revisited. In *Proc. IEEE Conf. on Computer Vision and Pattern Recognition (CVPR)*, 2016. 4, 10
- Hao Shao, Letian Wang, Ruobing Chen, Hongsheng Li, and Yu Liu. Safety-enhanced autonomous driving using interpretable sensor fusion transformer. In *Proc. Conf. on Robot Learning (CoRL)*, pp. 726–737, 2023. 2
- Peter Shaw, Jakob Uszkoreit, and Ashish Vaswani. Self-attention with relative position representations. In *Annual Conference of the North American Chapter of the Association for Computational Linguistics (NAACL-HLT)*, pp. 464–468, 2018. 1, 2
- Vincent Sitzmann, Semon Rezkikov, Bill Freeman, Josh Tenenbaum, and Fredo Durand. Light field networks: Neural scene representations with single-evaluation rendering. In *Advances in Neural Information Processing Systems (NeurIPS)*, pp. 19313–19325, 2021. 6
- Jianlin Su, Yu Lu, Shengfeng Pan, Ahmed Murtadha, Bo Wen, and Yunfeng Liu. Roformer: Enhanced transformer with rotary position embedding. *arXiv.org*, 2021. 5, 9
- Mohammed Suhail, Carlos Esteves, Leonid Sigal, and Ameesh Makadia. Generalizable patch-based neural rendering. In *Proc. of the European Conf. on Computer Vision (ECCV)*, pp. 156–174, 2022. 7
- Yutao Sun, Li Dong, Barun Patra, Shuming Ma, Shaohan Huang, Alon Benhaim, Vishrav Chaudhary, Xia Song, and Furu Wei. A length-extrapolatable transformer. In *ACL*, pp. 14590–14604, 2022. 9
- Mukund Varma, Peihao Wang, Xuxi Chen, Tianlong Chen, Subhashini Venugopalan, and Zhangyang Wang. Is attention all that nerf needs? In *Proc. of the International Conf. on Learning Representations (ICLR)*, 2023. 2
- Ashish Vaswani, Noam Shazeer, Niki Parmar, Jakob Uszkoreit, Llion Jones, Aidan N Gomez, Łukasz Kaiser, and Illia Polosukhin. Attention is all you need. In *NeurIPS*, volume 30, 2017. 1, 2
- Naveen Venkat, Mayank Agarwal, Maneesh Singh, and Shubham Tulsiani. Geometry-biased transformers for novel view synthesis. *arXiv.org*, 2023. 2
- Qianqian Wang, Zhicheng Wang, Kyle Genova, Pratul P Srinivasan, Howard Zhou, Jonathan T Barron, Ricardo Martin-Brualla, Noah Snavely, and Thomas Funkhouser. IBRNet: Learning multi-view image-based rendering. In *Proc. IEEE Conf. on Computer Vision and Pattern Recognition (CVPR)*, pp. 4690–4699, 2021. 2, 3, 7
- Xiaolong Wang, Ross B. Girshick, Abhinav Gupta, and Kaiming He. Non-local neural networks. In *Proc. IEEE Conf. on Computer Vision and Pattern Recognition (CVPR)*, pp. 7794–7803, 2018. 1, 2
- Daniel Watson, William Chan, Ricardo Martin-Brualla, Jonathan Ho, Andrea Tagliasacchi, and Mohammad Norouzi. Novel view synthesis with diffusion models. In *Proc. of the International Conf. on Learning Representations (ICLR)*, 2023. 2
- Daniel E Worrall, Stephan J Garbin, Daniyar Turmukhambetov, and Gabriel J Brostow. Interpretable transformations with encoder-decoder networks. In *Proc. of the IEEE International Conf. on Computer Vision (ICCV)*, pp. 5726–5735, 2017. 9
- Kan Wu, Houwen Peng, Minghao Chen, Jianlong Fu, and Hongyang Chao. Rethinking and improving relative position encoding for vision transformer. In *Proc. IEEE Conf. on Computer Vision and Pattern Recognition (CVPR)*, pp. 10033–10041, 2021. 2
- Haofei Xu, Jing Zhang, Jianfei Cai, Hamid Rezaatofghi, Fisher Yu, Dacheng Tao, and Andreas Geiger. Unifying flow, stereo and depth estimation. *IEEE Trans. on Pattern Analysis and Machine Intelligence (PAMI)*, 2023. 2
- Alex Yu, Vickie Ye, Matthew Tancik, and Angjoo Kanazawa. pixelnerf: Neural radiance fields from one or few images. In *Proc. IEEE Conf. on Computer Vision and Pattern Recognition (CVPR)*, 2021. 6, 7

Richard Zhang, Phillip Isola, Alexei A. Efros, Eli Shechtman, and Oliver Wang. The unreasonable effectiveness of deep features as a perceptual metric. In *Proc. IEEE Conf. on Computer Vision and Pattern Recognition (CVPR)*, pp. 586–595, 2018. [19](#)

Tinghui Zhou, Richard Tucker, John Flynn, Graham Fyffe, and Noah Snavely. Stereo magnification. *ACM Transactions on Graphics*, 37(4):1–12, 2018. [7](#)

A ALGORITHMIC DESCRIPTION OF GTA

Algorithm 1 provides an algorithmic description based on Eq. (6) for single-head self-attention. For multi-head attention, we simply apply the group representations to all QKV vectors of each head.

Algorithm 1 GTA for single head self-attention. The highlighted parts in red are new in GTA compared to the vanilla attention.

Input: Input tokens: $X \in \mathbb{R}^{N \times d}$, group representations: $\mathbf{P}_g = [\rho_{g_1}, \rho_{g_2}, \dots, \rho_{g_N}]$, and weights: $W^Q, W^K, W^V \in \mathbb{R}^{d \times d}$.

1. Compute query, key, and value from X : $Q = XW^Q, K = XW^K, V = XW^V$
2. Transform each variable with the group representations:

$$Q \leftarrow \mathbf{P}_g^T \odot Q, K \leftarrow \mathbf{P}_g^{-1} \odot K, V \leftarrow \mathbf{P}_g^{-1} \odot V$$

3. Compute QKV attention in the same way as in the vanilla attention:

$$O = \text{softmax} \left(\frac{QK^T}{\sqrt{d}} \right) V$$

4. Apply group representations to O :

$$O \leftarrow \mathbf{P}_g \odot O$$

5. Return O
-

Computational complexity Since the $\mathbf{P}_g \odot \cdot$ operation is n -times multiplication of a $d \times d$ matrix with a d -dimensional vector, the computational complexity of additional computation for our attention over the vanilla attention is $O(nd^2)$. This can be reduced by constructing the representation matrix with a block diagonal, with each block being small. If we keep the largest block size of the representation constant against n and d , then the order of the $\mathbf{P}_g \odot \cdot$ operation becomes $O(nd)$. Thus, if d_{\max} is relatively small, or if we increase n or d , the computation overhead of the \odot operation becomes negligible compared to the computation times of the other components of a transformer, which are $O(n^2d)$ for attention and $O(nd^2)$ for feedforward layers. In our actual experiments, we use a block-structured representation with a maximum block size of 5 (see Section 3.2 and Fig. 8).

B DETAILS OF THE SYNTHETIC EXPERIMENTS IN SECTION 3.1

We use 10,000 training and test scenes. For the intrinsics, both the vertical and horizontal sensor width are set to 1.0, and the focal length is set to 4.0, leading to an angle of view of 28° .

For optimization, we use AdamW (Loshchilov & Hutter, 2017) with weight decay 0.001. For each positional encoding method, we trained multiple models with different learning rates of $\{0.0001, 0.0002, 0.0005\}$ and found 0.0002 to work best for all models, and hence show results with this learning rate. We use three attention layers for both the encoder and the decoder. The image feature dimension is $32 \times 32 \times 3$. This feature is flattened and fed into a 2 layer-MLP to be transformed into the same dimensions as the token dimension d . We also apply a 2 layer-MLP to the output of the decoder to obtain the 3,072 dimensional predicted image feature. The token dimensions d are set to 512 for APE and RPE. As we mention in the descriptions of the synthetic experiment, ρ_g is composed of block concatenation of 3×3 rotation matrices, and we set d to 510 for GTA, which is divisible by 3. Note that there is no difficulty with the case where d is not divisible by 3. In that case, we can apply ρ_g only to certain components of vectors whose dimensions are divisible by 3 and apply no transformation to the other dimensions. This corresponds to applying a trivial representation, i.e., the identity matrix, to the remaining vectors.

The RPE-based model we designed is a sensible model. For example, if $b^Q = b^K$ and the set of three-dimensional vector blocks of b^Q forms an orthonormal basis, then the inner product of the

transformed query and key bias vectors becomes the *trace* of the product of the rotation matrices: $\langle \rho(r)b^Q, \rho(r')b^K \rangle = \text{tr}(R^T R')$. $\text{tr}(A^T B)$ is a natural inner product for matrices, by which we can bias the attention weight based on the inner-product-based similarity of matrices. Hence, we initialize each of the biases with vectorized identity matrices.

C DETAILS OF THE REPRESENTATION MATRICES

ρ_g is composed of four different types of representations $\rho_c, \rho_r, \rho_{\theta_h}, \rho_{\theta_w}$ with the multiplicities of s, t, u, v . Below, we describe the details of each representation.

$\sigma_{\text{cam}}(c)$: We use a homogenous rigid transformation as the representation of $c \in SE(3)$:

$$\sigma_{\text{cam}}(c) := \begin{bmatrix} R & T \\ 0 & 1 \end{bmatrix} \in \mathbb{R}^{4 \times 4}. \quad (9)$$

$\sigma_{\text{rot}}(r)$: We compose $\sigma_{\text{rot}}(r)$ via block concatenation of Wigner-D-matrices (Chirikjian, 2000).

$$\sigma_{\text{rot}}(r) := \bigoplus_k \sigma_{\text{rot}}^{(l_k)}(r), \quad \sigma_{\text{rot}}^{(l)}(r) := D_r^{(l)} \in \mathbb{R}^{(2l+1) \times (2l+1)} \quad (10)$$

where $D_r^{(l)}$ is l -th Wigner-D-matrix given r . Here, $\bigoplus_{a \in S} A^{(a)} := A^{(a_1)} \oplus \dots \oplus A^{(a_{|S|})}$ and we omit the index set symbol from the above equation. We use these matrices because Wigner-D-matrices are the *only irreducible representations* of $SO(3)$. Any linear representation $\sigma_r, r \in SO(3)$ is equivalent to a direct sum of the matrices under a similarity transformation (Chirikjian, 2000).

$\sigma_h(\theta_h)$ and $\sigma_w(\theta_w)$: Similar to $\sigma_{\text{rot}}(r)$, we use 2D rotation matrices with different frequencies for $\sigma_h(\theta_h)$ and $\sigma_w(\theta_w)$. Specifically, for $\sigma_h(\theta_h)$ given a set of frequencies $\{f_k\}_{k=1}^{N_h}$, we define the representation as follows:

$$\sigma_h(\theta_h) := \bigoplus_k \sigma_h^{(f_k)}(\theta_h), \quad \sigma_h^{(f)}(\theta_h) := M_{\theta_h}^{(f)} = \begin{bmatrix} \cos(f\theta_h) & -\sin(f\theta_h) \\ \sin(f\theta_h) & \cos(f\theta_h) \end{bmatrix} \in \mathbb{R}^{2 \times 2}. \quad (11)$$

$\sigma_w(\theta_w)$ is defined analogously.

We use the following strategy to choose the multiplicities s, t, u, v and frequencies $\{l\}, \{f_h\}, \{f_w\}$:

1. Given the feature dimension d of the attention layer, we split the dimensions into three components based on the ratio of $2 : 1 : 1$.
2. • We apply $\sigma_{\text{cam}}^{\oplus s}$ to the first half of the dimensions. As σ_{cam} does not possess multiple frequencies, its multiplicity is set to $d/8$.
 - $\sigma_{\text{rot}}^{\oplus r}$ is applied to a quarter of the dimensions. For the frequency parameters $\{l\}$ of σ_{rot} , we consistently use the 1st and 2nd degrees of the Wigner-D matrices. Considering the combined sizes of these matrices is 8, the multiplicity for σ_{rot} becomes $d/32$.
 - For the remaining $1/4$ of the dimensions of each QKV vector, we apply both $\sigma_h^{\oplus t}$ and $\sigma_w^{\oplus u}$. Regarding the frequency parameters $\{f_h\}, \{f_w\}$, we utilize $d/8$ octaves with the maximum frequency set at 1 for both σ_h and σ_w . The multiplicities for these are both 1.

Based on this strategy, we use the multiplicities and frequencies shown in Table 6.

D EXPERIMENTAL SETTINGS

Table 7 shows dataset properties and hyperparameters that we use in our experiments. We train with 4 RTX 2080 Ti GPUs on CLEVR-TR and with 4 Nvidia A100 GPUs on the other datasets.

CLEVR-TR and MSN-Hard CLEVR-TR is synthesized by using Kubric (Greff et al., 2022). The resolution of each image is 240×320 . The camera poses of the dataset include translation, azimuth, and elevation transformations. The camera does not always look at the center of the scene.

MSN-Hard is also a synthetically generated dataset. Up to 32 objects sampled from ShapeNet (Chang et al., 2015) appear in each scene. All 51K ShapeNet objects are used for this dataset, and the training and test sets do not share the same objects with each other. MSN-Hard

Table 6: **Multiplicity and frequency parameters.** Here, d is the dimensions of each attention head. Since the baseline model on RealEstate10k and ACID uses different feature sizes for query-key vectors and value vectors, we also use different sizes of representation matrices for each feature.

	d	$\{s, t, u, v\}$	$\{l_1, \dots, l_{N_{\text{rot}}}\}$	$\{f_1, \dots, l_{N_{\{h,w\}}}\}$
CLEVR-TR	64	$\{8, 3, 1, 1\}$	$\{1, 2\}$	$\{1, \dots, 1/2^3\}$
CLEVR-TR wo/ $SO(3)$		$\{8, 0, 1, 1\}$	—	$\{1, 1/2, 1/4, \dots, 1/2^7\}$
MSH-Hard	96	$\{12, 3, 1, 1\}$	$\{1, 2\}$	$\{1, 1/2, 1/4, \dots, 1/2^5\}$
MSH-Hard wo/ $SO(3)$		$\{12, 0, 1, 1\}$	—	$\{1, 1/2, 1/4, \dots, 1/2^{11}\}$
Realestate10k and ACID (Encoder)	64	$\{8, 3, 1, 1\}$	$\{1, 2\}$	$\{1, \dots, 1/2^3\}$
Realestate10k and ACID (Decoder, key)	128	$\{16, 6, 1, 1\}$	$\{1, 2\}$	$\{1, \dots, 1/2^7\}$
Realestate10k and ACID (Decoder, value)	256	$\{32, 12, 1, 1\}$	$\{1, 2\}$	$\{1, \dots, 1/2^{15}\}$

Table 7: **Dataset properties and architecture hyperparameters.** # target pixels indicate how many query pixels are sampled for each scene during training. *We use 12 heads for the attention layers in SRT and 8 heads in RePAST and GTA because 12 head models do not fit into our GPU memory with those methods. †The decoder’s attention layers only have a single head. Also, the token dimensions in the decoder are set to 128 for query-key vectors and 256 for value vectors.

dataset	CLEVR-TR	MSN-Hard	RealEstate10k	ACID
# Training scenes	20,000	1,000,000	66,837	10,974
# Test scenes	1,000	10,000	7,192	1,910
Batch size	32	64	48	48
Training steps	2,000,000	4,000,000	300,000	200,000
Learning rate	1e-4	1e-4	5e-4	
# Context views	2	5	2	
# Target pixels	512	2,048	192	
# Self-attention layers in the encoder	5	5	12	
# Cross-attention layers in the decoder	2	2	2	
# Heads in attention layers	6	12/8*	12†	
Token dimensions	384	768	768†	
MLP dimensions	768	1,536	3,072	

includes instance masks for each object in a scene, which we use to compute the attention matrix alignment score described in Section 4 and Appendix E.3. The resolution of each image is 128×128 .

We basically follow the same architecture and hyperparameters of the improved version of SRT described in the appendix of Sajjadi et al. (2022a), except that we use AdamW (Loshchilov & Hutter, 2017) with the weight decay set to the default parameter and dropout with a ratio of 0.01 at every attention output and hidden layers of feedforward MLPs.

Since there is no official code or released models available for SRT and RePAST, we train both baselines ourselves and obtain almost comparable but slightly worse results (Table 8). This is because we train the models with a smaller batch size and target ray samples than in the original setting due to our limited computational resources (4 A100s). Note that our model, which is also trained with a smaller batch size, still outperforms the original SRT and RePAST models scores.

RealEstate10k and ACID Both datasets are sampled from videos available on YouTube. At the time we conducted our experiments, some of the scenes used in Du et al. (2023) were no longer available on YouTube. We used scenes 66,837 and 10,974 training scenes and 7,192 and 1,910 test scenes for RealEstate10k and ACID, respectively. The resolution of each image in the original sequences is 360×640 . For training, we apply downsampling followed by a random crop and random horizontal flipping to each image, and the resulting resolution is 256×256 . For test time, we apply downsampling followed by a center crop to each image. The resolution of each processed image is also 256×256 . We follow the same architecture and optimizer hyperparameters of Du et al. (2023). Although the authors of Du et al. (2023) released the training code and their model on

Table 8: **Performance comparison between numbers reported in Safin et al. (2023) and our reproduced numbers.** Note that Safin et al. (2023) uses 4x larger batch size than available in our experimental setting (4 A100s). The iteration for which we train each model is the same as Safin et al. (2023).

	PSNR \uparrow	LPIPS $_{\text{VGG}/\text{Alex}}\downarrow$	SSIM \uparrow
SRT (Sajjadi et al., 2022b)	24.56	NA/0.223	0.784
RePAST (Safin et al., 2023)	24.89	NA/0.202	0.794
SRT	24.27	0.368/0.279	0.741
RePAST	24.48	0.348/0.243	0.751
GTA (Ours)	25.72	0.289/0.185	0.798

Table 9: **Comparison between results reported in Du et al. (2023) (Top) and our reproduced results (Bottom).**

	RealEstate10k			ACID		
	PSNR \uparrow	LPIPS \downarrow	SSIM \uparrow	PSNR \uparrow	LPIPS \downarrow	SSIM \uparrow
Du et al. (2023)	21.38	0.262	0.839	23.63	0.364	0.781
Du et al. (2023)	21.65	0.284	0.822	23.35	0.334	0.801
GTA (Ours)	22.85	0.255	0.850	24.10	0.291	0.824

RealEstate10k, we observed that the model produces worse results than those reported in their work. The results were still subpar even when we trained models with their code. As a result, we decided to train each model with more iterations (300K) compared to the 100K iterations mentioned in their paper and achieved comparable scores on both datasets. Consequently, we also trained GTA-based models for 300K iterations as well.

D.1 SCENE REPRESENTATION TRANSFORMER (SRT)

Encoding views: Let us denote N_{context} -triplets of input view images and their associated camera information by $\mathbf{I} := \{(I_i, c_i, M_i)\}_{i=1}^{N_{\text{context}}}$, where N_{context} is the number of context views, $I_i \in \mathbb{R}^{H \times W \times 3}$ is the i -th input RGB image, and $c_i \in \mathbb{R}^{4 \times 4}$, $M_i \in \mathbb{R}^{3 \times 3}$ are a camera extrinsic and a camera intrinsic matrix associated of the i -th view. The SRT encoder E encodes the context of views into scene representation S and is composed of a CNN and a transformer $E_{\text{transformer}}$. First, a 6-layer CNN E_{CNN} is applied to a ray-concatenated image I' of each view to obtain $(H/D) \times (W/D)$ -

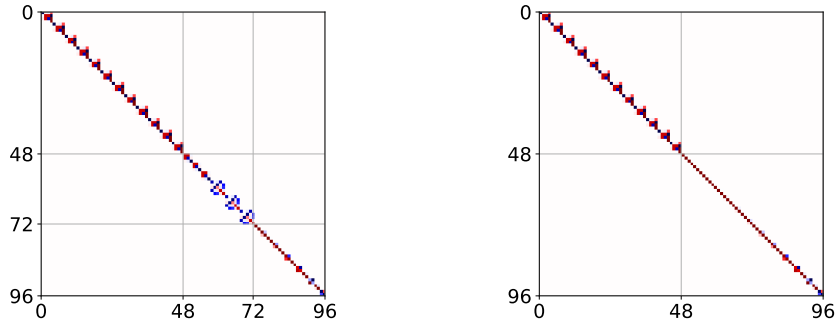


Figure 8: **Representation matrices on MSN-Hard.** Left: with $SO(3)$, Right: without $SO(3)$. Left: Dimensions 1-48 correspond to $\sigma_{\text{cam}}^{\oplus 12}(c)$, dimensions 49-72 correspond to $\sigma_{\text{rot}}^{\oplus 3}(r)$, and dimensions 73-96 correspond to $\sigma_h(\theta_h)$ and $\sigma_w(\theta_w)$. Right: Dimensions 1-48 correspond to $\sigma_{\text{cam}}^{\oplus 12}(c)$ and dimensions 49-96 correspond to $\sigma_h(\theta_h)$ and $\sigma_w(\theta_w)$.

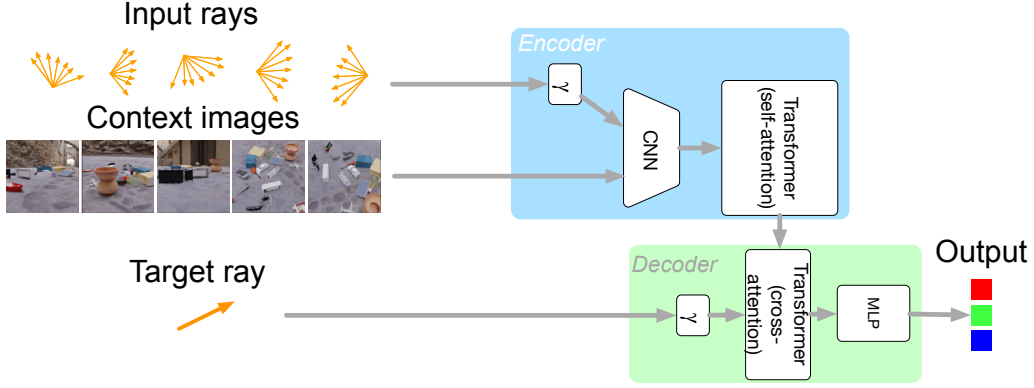


Figure 9: **Scene representation transformer (SRT) rendering process.** The encoder E consisting of a stack of convolution layers followed by a transformer encoder translates context images into a set representation S . The decoder D predicts an RGB pixel value given a target ray and S . In our model, every attention layer in both the encoder and decoder is replaced with GTA. We also remove the input and target ray embeddings from the input of the encoder and decoder, respectively. We input a learned constant vector to the decoder instead of the target ray embeddings.

resolution features:

$$F_i = E_{\text{CNN}}(I'_i) \in \mathbb{R}^{(H/D) \times (W/D) \times d}, I'_{ihw} = I_{ihw} \oplus \gamma(r_{ihw}) \quad (12)$$

where d is the output channel size of the CNN, and D is the downsampling factor, which is set to 8. γ is a harmonic embedding function that transforms ray $r = (o, d) \in \mathbb{R}^3 \times \mathcal{S}$ into a concatenation of the Fourier features with multiple frequencies. Each ray r_{ihw} is computed from given camera's extrinsic and intrinsic parameters (c_i, M_i) . Here, " \oplus " denotes vector concatenation.

Next, a transformer-based encoder $E_{\text{transformer}}$ processes the flattened CNN features of all views together to output the scene representation:

$$S := \{s_i\}_{i=1}^{N_{\text{context}} * (H/D) * (W/D)} = E_{\text{transformer}} \left(\{f_i\}_{i=1}^{N_{\text{context}} * (H/D) * (W/D)} \right) \quad (13)$$

where $\{f_i\}$ is the set of flattened CNN features.

Rendering a view: Given the scene representation S and a target ray r^* , the decoder D outputs an RGB pixel:

$$\hat{a}_{r^*} = D(\gamma(r^*), S) \in \mathbb{R}^3. \quad (14)$$

where γ is the same function used in Eq. (12). The architecture of D comprises two stacks of a cross-attention block followed by a feedforward MLP. The cross-attention layers determine which token in the set S to attend to, to render a pixel corresponding to the given target ray. The output of the cross-attention layers is then processed by a 4-layer MLP, to get the final RGB prediction. The number of hidden dimensions of this MLP is set to 1536.

Optimization: The encoder and the decoder are optimized by minimizing the mean squared error between given target pixels a_{r^*} and the predictions:

$$\mathcal{L}(E, D) = \sum_{r^*} \|a_{r^*} - \hat{a}_{r^*}\|_2^2. \quad (15)$$

D.2 DETAILS OF THE ARCHITECTURE AND LOSS OF DU ET AL. (2023)

Du et al. (2023) proposes an SRT-based transformer NVS model with a sophisticated architecture. The major differences between their model and SRT are that they use a dense vision transformer (Ranftl et al., 2021) for their encoder. They also use an epipolar-based sampling technique to select context view tokens, a process that helps render pixels efficiently in the decoding process.

Table 10: **Test metrics on CLEVR-TR.**

	PSNR \uparrow	LPIPS \downarrow	SSIM \uparrow
APE	33.66	0.161	0.960
RPE	36.06	0.159	0.971
SRT	33.51	0.158	0.960
RePAST	37.27	0.119	0.977
GTA (Ours)	39.63	0.108	0.984

We use the same optimization losses for training models based on this architecture as [Du et al. \(2023\)](#). Specifically, we use the L_1 loss between target and predicted pixels on RealEstate10k and ACID. We also use the following combined loss after the 30K-th iterations on ACID.

$$L_1(P, \hat{P}) + \lambda_{\text{LPIPS}} L_{\text{LPIPS}}(P, \hat{P}) + \lambda_{\text{depth}} L_{\text{depth}}(P, \hat{P}) \quad (16)$$

where $P, P' \in \mathbb{R}^{32 \times 32 \times 3}$ are target and predicted patches. L_{LPIPS} is the perceptual similarity metric proposed by [Zhang et al. \(2018\)](#). L_{depth} is a regularization loss that promotes the smoothness of estimated depths in the model. Please refer to [Du et al. \(2023\)](#) for more details. On RealEstate10k, we found that using the combined loss above deteriorates reconstruction metrics. Therefore, we train models on RealEstate10k solely with the L_1 loss for 300K iterations.

D.3 APE- AND RPE-BASED TRANSFORMERS ON CLEVR-TR

For the APE-based model, we replace the ray embeddings in SRT with a linear projection of the combined 2D positional embedding and flattened $SE(3)$ matrix. To build an RPE-based model, we follow the same procedure as in Section 3.1 and apply the representations to the bias vectors appended to the QKV vectors. Each bias dimension is set to 16 for the σ_{cam} and 16 for σ_h and σ_w . The multiplicities and frequency parameters are determined as described in Section 3.2. $\{s, u, v\}$ is set to $\{4, 1, 1\}$ and $\{f\}$ is set to $\{1, \dots, 1/2^3\}$ for both σ_h and σ_w . Table 10 shows an extended version of Table 2, which includes LPIPS ([Zhang et al., 2018](#)) and SSIM performance.

E ADDITIONAL EXPERIMENTAL RESULTS

E.1 PERFORMANCE WITH DIFFERENT RANDOM SEEDS

We observe that the performance variance of different random weight initializations is quite small, as shown in Fig. 10, which displays the mean and standard deviation across 4 different seeds. We see that the variance is relatively insignificant compared to the performance difference between the compared methods. Consequently, the results reported above are statistically meaningful.

E.2 PERFORMANCE DEPENDENCE ON THE REFERENCE COORDINATES

Table 11 highlights the importance of coordinate-choice invariance. ‘‘SRT (global coord)’’ is trained with camera poses that have their origin set to always be in the center of all objects. This setting enables the model to know how far the ray origin is from the center of the scene, therefore enabling the model to easily find the position of the surface of objects that intersect with the ray. We see that SRT’s performance heavily depends on the choice of reference coordinate system. Our model is, by construction, invariant to the choice of coordinate system and outperforms even the privileged version of SRT.

E.3 ANALYSIS OF ATTENTION PATTERNS

We conducted an analysis on the attention matrices of the encoders trained on MSN-Hard. We found that the GTA-based model tends to attend to features of different views more than RePAST, which we show in Fig. 11. Furthermore, we see that GTA not only correctly attends to the respective patches of different views, but also can attend to object level regions (Fig. 7 and 12). Surprisingly, these attention patterns are seen at the very beginning of the course of the encoding process: the

Table 11: **Test PSNRs in a setting where global coordinates are shared across scenes.** All numbers show test PSNRs and are produced with models trained for 1M iterations. Note that GTA is invariant to the reference coordinates of the extrinsics, and the performance is not affected by the choice of the reference coordinate system.

Method	CLEVR-TR	MSH-Hard
SRT	32.97	23.15
SRT (global coord)	37.93	24.20
GTA wo $SO(3)$	38.99	24.58

Table 12: **Computational time to perform one gradient step, encode a single scene, and render a single entire image on MSN-Hard (top) and RealEstate10K (bottom).** All time values are expressed in milliseconds (ms). As for one gradient step time, we only measure time for forward-backward props and weight updates and exclude data loading time. We measure each time on a single A100 with bfloat16 precision for MSN-Hard and float32 precision for RealEstate10k.

Method	One gradient step	Encoding	Rendering
SRT	296	5.88	16.4
RePAST	394	7.24	21.4
GTA	379	17.7	20.9

Method	One gradient step	Encoding	Rendering
Du et al. (2023)	619	49.8	1.42×10^3
GTA	806	74.3	2.05×10^3

visualized attention maps are obtained in the 2nd attention layer. To evaluate how well the attention maps α weigh respective object features across views, we compute a retrieval-based metric with instance segmentation masks of objects provided by MSN-Hard. Specifically, given a certain layer’s attention maps α :

1. We randomly sample the i -th query patch token with 2D position $p \in \{1, \dots, 16\} \times \{1, \dots, 16\}$.
2. We compute the attention map $\bar{\alpha}_i \in [0, 1]^{5 \times 16 \times 16}$ averaged over all heads.
3. We then identify which object belongs to that token’s position by looking at the corresponding 8×8 region of the instance masks. Note that multiple objects can belong to the region.
4. For each belonging object, we compute precision and recall values with $\mathbb{1}[\bar{\alpha}_i > t]$ as prediction and 0–1 masks of the corresponding object as ground truth on all context views, by changing the threshold value $t \in [0, 1]$.
5. In the final step, we calculate a weighted average of the precision and recall values for each object. To determine the weight of each object, we consider the number of pixels assigned to that object’s mask within the 8×8 region. We then normalize these weights so that their sum equals to be one.

We collect multiple precision and recall values by randomly sampling scenes and patch positions 2000 times and then compute the average of the collected precision-recall curves. In Fig. 13, we show averaged precision-recall curves. Table 7 shows the area under the precision-recall curves (PR-AUCs) of each layer. We see that the GTA-based model learns well-aligned attention maps with the ground truth object masks for every layer.

E.4 COMPUTATIONAL TIME

We measure the time to perform one-step gradient descent, as well as encoding and decoding for each method. Table 12 shows that the computational overhead added by the use of GTA is comparable to RePAST on MSN-Hard. In contrast to GTA and RePAST-based models which encode positional information into every layer, SRT and [Du et al. \(2023\)](#) add positional embeddings only to each encoder and decoder input. As a result, the computational time of SRT for one-step gradient

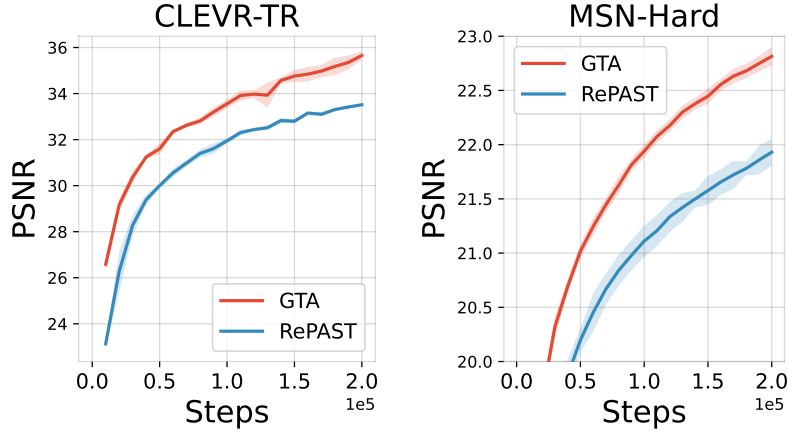


Figure 10: **Mean and standard deviation plots of validation PSNRs on CLEVR-TR and MSN-Hard.** Due to the heavy computation requirements for training, we only trained models with 200,000 iterations and measured the validation PSNRs during the course of the training.

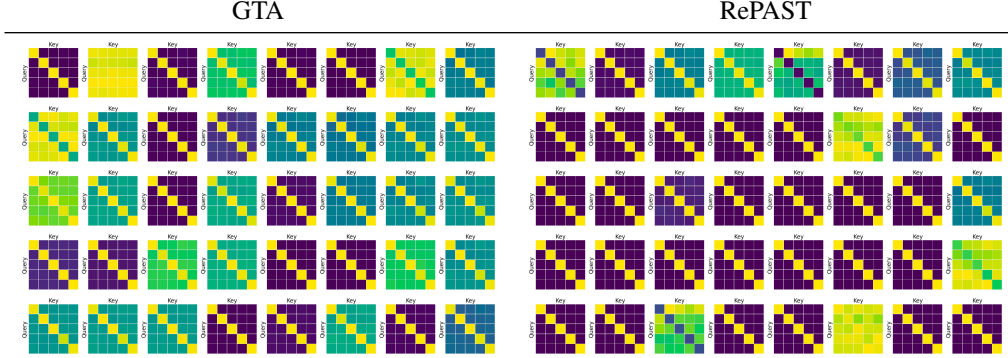


Figure 11: **Visualization of view-to-view attention maps.** The (i, j) -th element of each 5×5 matrix represents the average of attention weights between all pairs of each query token of the i -th context view and each key token of the j -th context view. The (l, m) -th panel shows the weight of the m -th head at the l -th layer. Yellow and dark purple cells indicate high and low attention weight, respectively. A matrix with high diagonal values means that the corresponding attention head attends *within each view* while with high non-diagonal values means the corresponding attention head attends *across views*.

descent is around 1.3x faster than RePAST and GTA, and that of [Du et al. \(2023\)](#) is 1.3x faster than GTA.

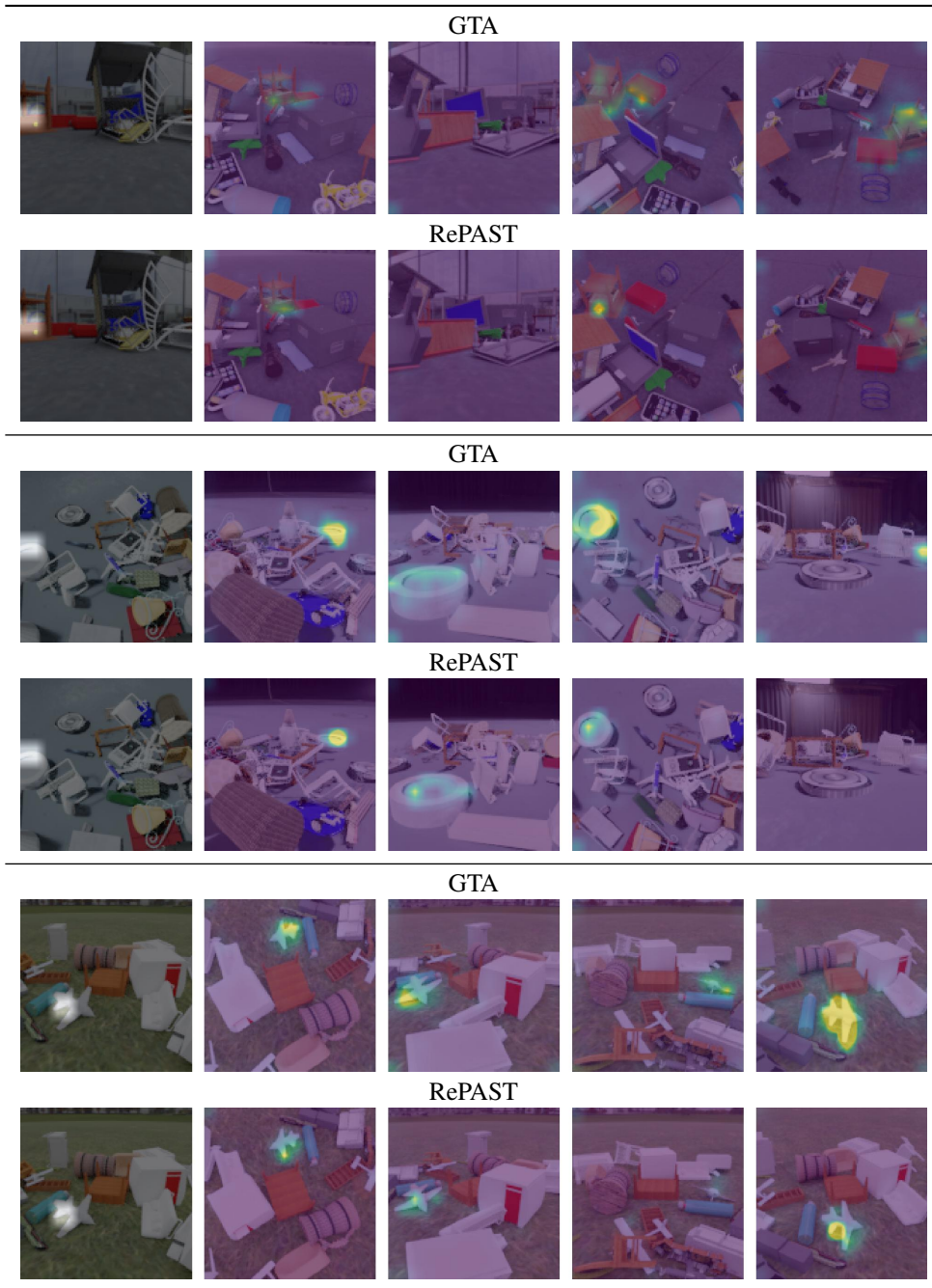


Figure 12: Additional attention map visualizations.

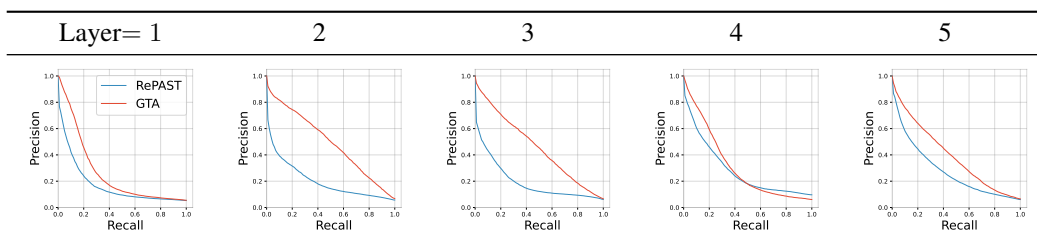


Figure 13: Precision-recall curves of the attention matrices of each encoder layer.

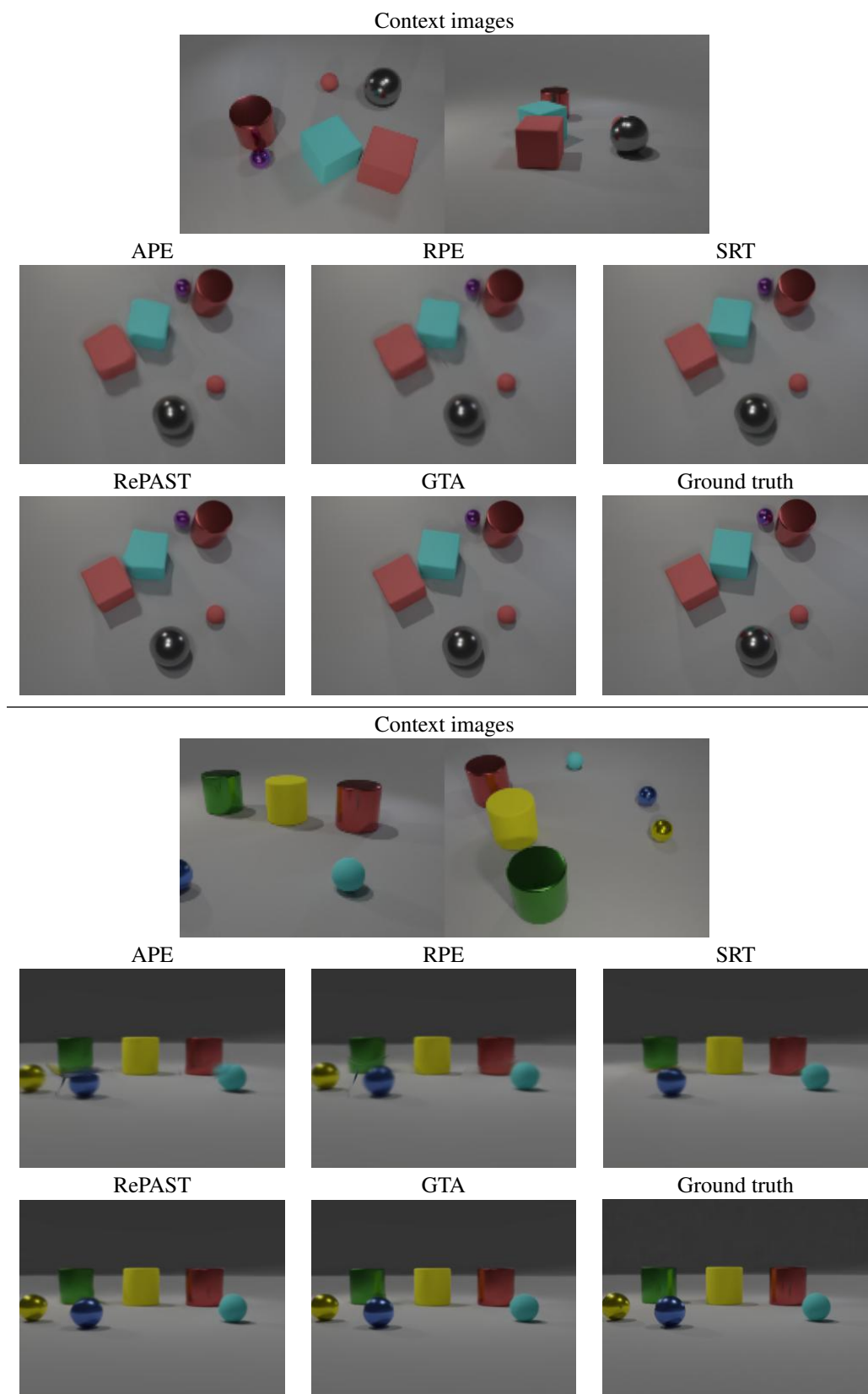


Figure 14: **Qualitative results on CLEVR-TR.**

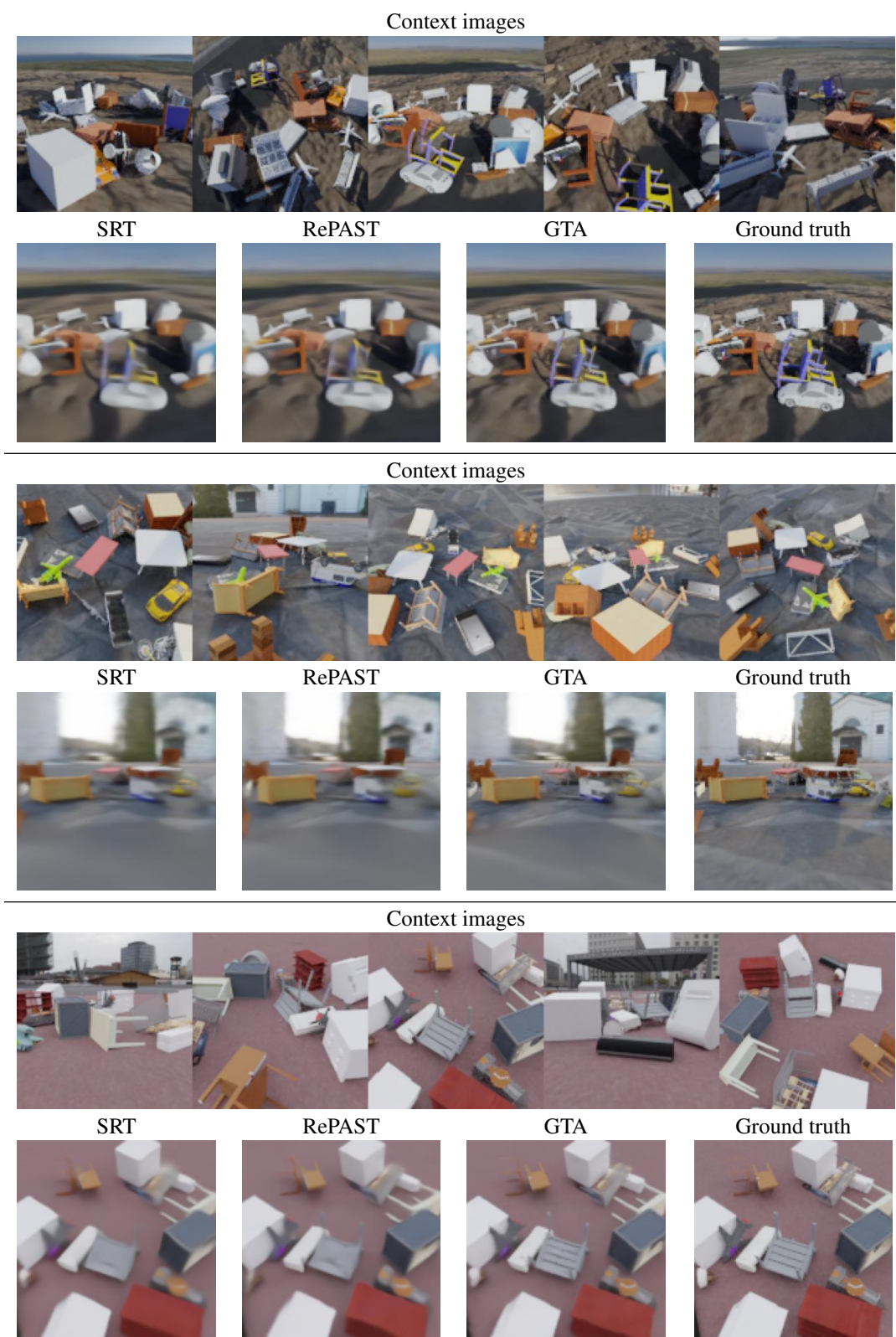


Figure 15: **Qualitative results on MSN-Hard.**

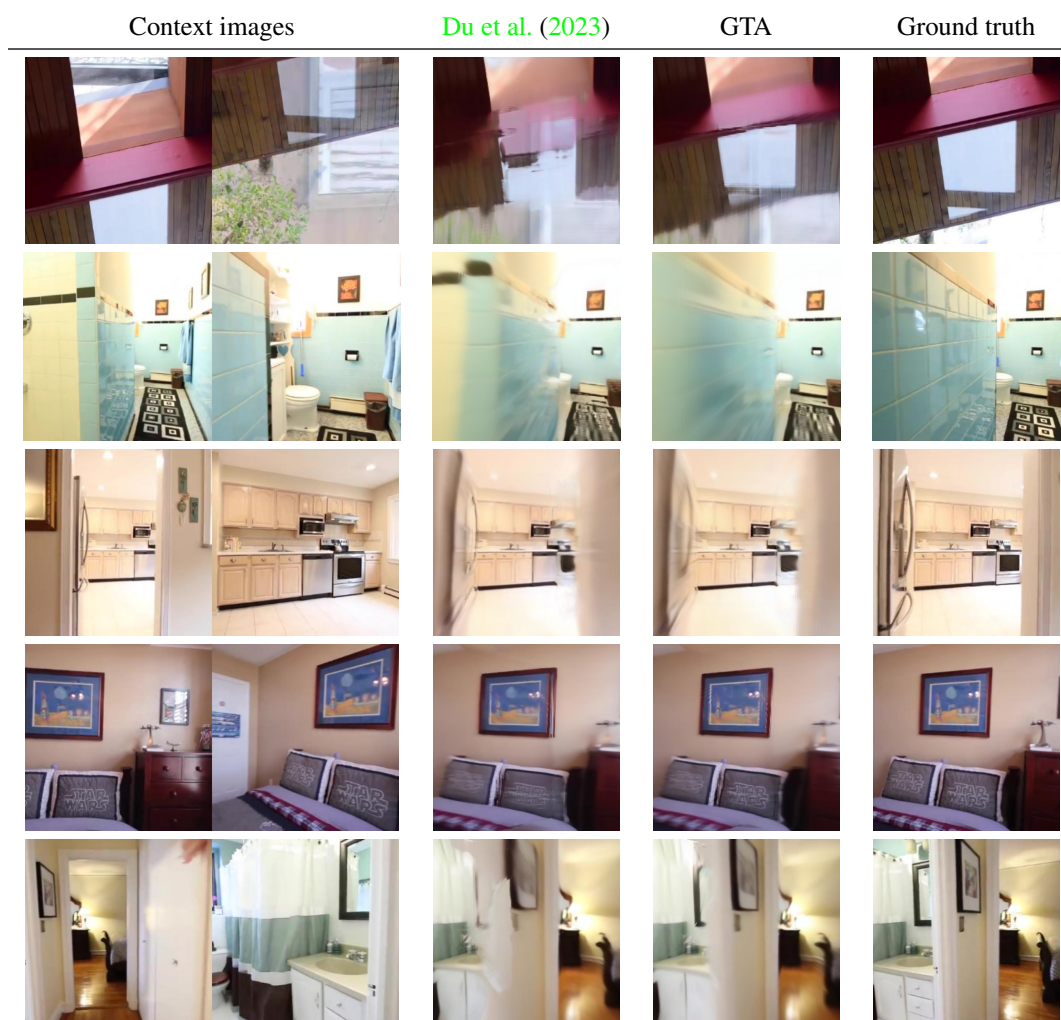


Figure 16: Qualitative results on RealEstate10k.

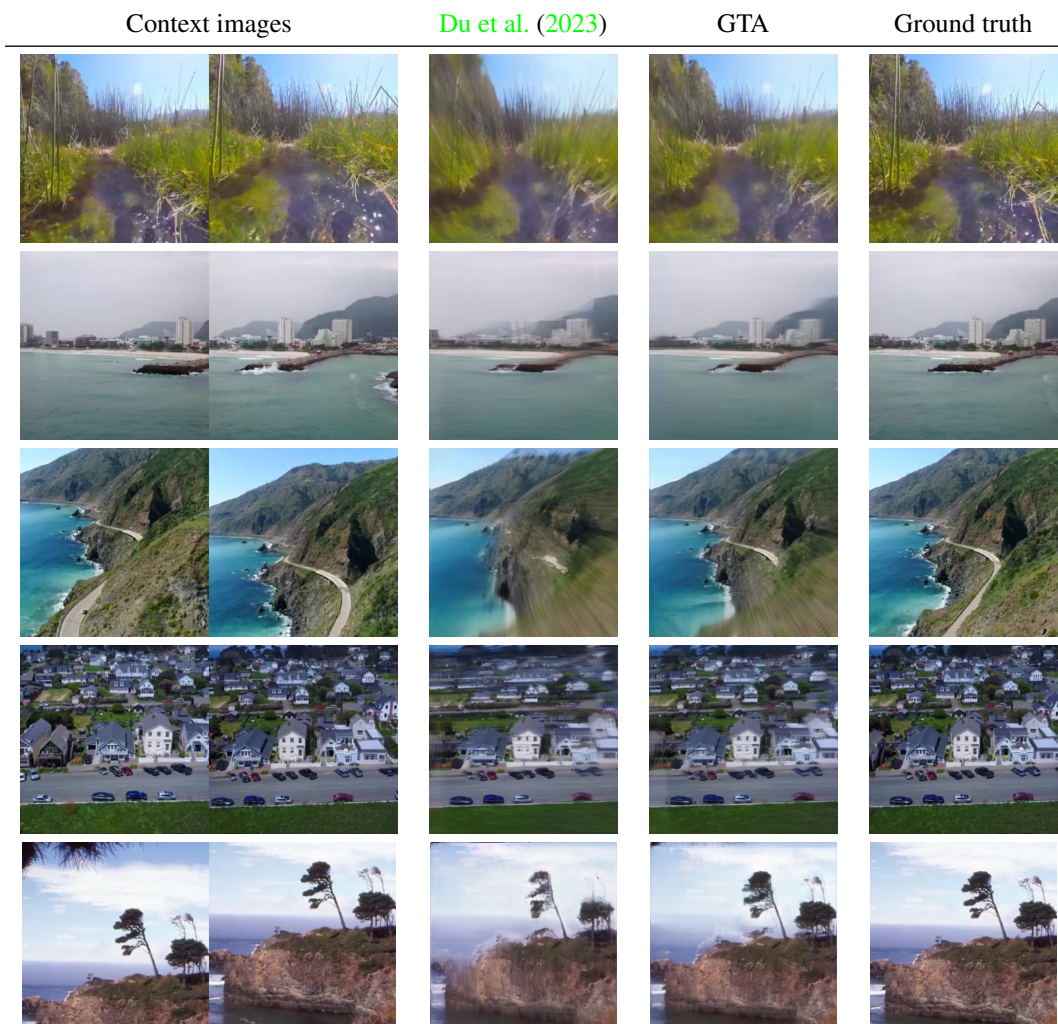


Figure 17: Qualitative results on ACID.